Electronic Supplementary Information

Supported ε and β iron oxide nanomaterials by chemical vapor deposition: structure, morphology and magnetic properties

Giorgio Carraro,[a] *Davide Barreca,*[*b] *Chiara Maccato,*[a] *Elza Bontempi,*[c] *Laura E. Depero,*[c] *César de Julián Fernández,*[d] *and Andrea Caneschi*[*e]

[a] Department of Chemistry, Padova University and INSTM, via F. Marzolo, 1, 35131 Padova, Italy

[b] CNR-ISTM and INSTM, Department of Chemistry - Padova University, via F. Marzolo, 1, 35131 Padova, Italy

[c] Chemistry for Technologies Laboratory, Brescia University and INSTM, via Branze, 38, 25123 Brescia, Italy

[d] CNR-ISTM and INSTM, via C. Golgi, 19, 20133 Milano, Italy

[e] Department of Chemistry, Florence University and INSTM, via della Lastruccia, 3, 50019 Sesto Fiorentino (FI), Italy

[*] Authors to whom correspondence should be addressed; e-mail: davide.barreca@unipd.it (D.B.); andrea.caneschi@unifi.it (A.C.).

Experimental

A cold-wall horizontal CVD apparatus was adopted for the synthesis of iron oxide systems, using $Fe(hfa)_2$•TMEDA as a molecular source (hfa = 1,1,1,5,5,5 - hexafluoro - 2,4 - pentanedionate; TMEDA = *N*,*N*,*N'*,*N'* – tetramethylethylenediamine; vaporization temperature = 333 K).[R1,R2] Growth temperature and pressure were set at 673 K, 10 mbar (ε-Fe_2O_3) and 773 K, 3 mbar (β-Fe_2O_3). Precursor vapors were transported towards the deposition zone by an O_2 flow (purity = 6.0; rate = 100 and 20 sccm for ε-Fe_2O_3 and β-Fe_2O_3, respectively) through gas lines heated at 393 K. In the case of ε-Fe_2O_3, an auxiliary oxygen flow (100 sccm) was introduced separately into the reaction chamber after passing through a water reservoir maintained at 323 K. Depositions were carried out for a total duration of 60 min on *p*-type Si(100) substrates (MEMC®, Merano, Italy, 10 mm × 10 mm × 1 mm), subjected to an established pre-cleaning procedure aimed at removing surface contamination.[R3]

XRD^2 images were collected by a Dymax-RAPID X-ray microdiffractometer, with a cylindrical imaging plate detector, that allows collecting diffraction data in the ranges 2θ = 0 – 160° (horizontally) and 2θ = -45 – +45° (vertically) upon using CuKα radiation. The incident beam collimators enable different spot sizes to be projected onto the sample. In this work, measurements were made in reflection mode, adopting a collimator diameter of 300 μm and an exposure time of 30 min for each XRD^2 pattern.

FE-SEM micrographs were collected by a Zeiss SUPRA 40VP instrument, with primary beam voltages between 10 and 20 kV.

XPS analyses were carried out by a Perkin-Elmer Φ5600ci spectrometer at pressures lower than 1×10^{-8} mbar, using a non-monochromatized AlKα source (hν = 1486.6 eV). After a Shirley-type

background subtraction, raw XPS spectra were fitted by a nonlinear least-squares deconvolution adopting Gaussian-Lorentzian peak shapes. The reported BEs (standard deviation = ± 0.2 eV) were corrected for charging effects by assigning to the C1s line of adventitious carbon a position of 284.8 eV.

Magnetic measurements were performed using a SQUID magnetometer (Quantum Design MPMS) operating in the 3.0 – 300 K temperature range, with an applied field up to 50 kOe. Magnetic moments of the investigated systems were obtained by subtracting the Si(100) diamagnetic contribution, that was independently measured on a bare substrate of the same dimensions. The magnetic moment was normalized to the system geometrical area.

Structural characterization: XRD[2] analysis

In Figs. 1a and S1a, the peaks located at 2ϑ = 27.6°, 29.9°, 32.8°, 35.2°, 36.4°, 37.9°, 40.1°, 41.3°, 45.2°, 45.7°, 49.2°, 52.9°, 61.1°, 62.7° and 65.9° can be assigned respectively to the (112), (013), (122), (200)/(130), (201), (211)/(004), (202)/(132), (212), (222), (203)/(133), (142)/(015), (204)/(134), (205)/(135), (116), (323) reflections of orthorhombic ε-Fe_2O_3.[R4]

In Figs. 1b and S1b, the peaks at 2ϑ = 23.1°, 32.9°, 38.2°, 40.6°, 45.1°, 49.4°, 55.2°, 60.7°, 64.1°, 65.8 and 67.4° can be attributed respectively to the (211), (222), (400), (411), (332), (431), (440), (611), (541), (622) and (631) reflections of cubic β-Fe_2O_3.[R5]

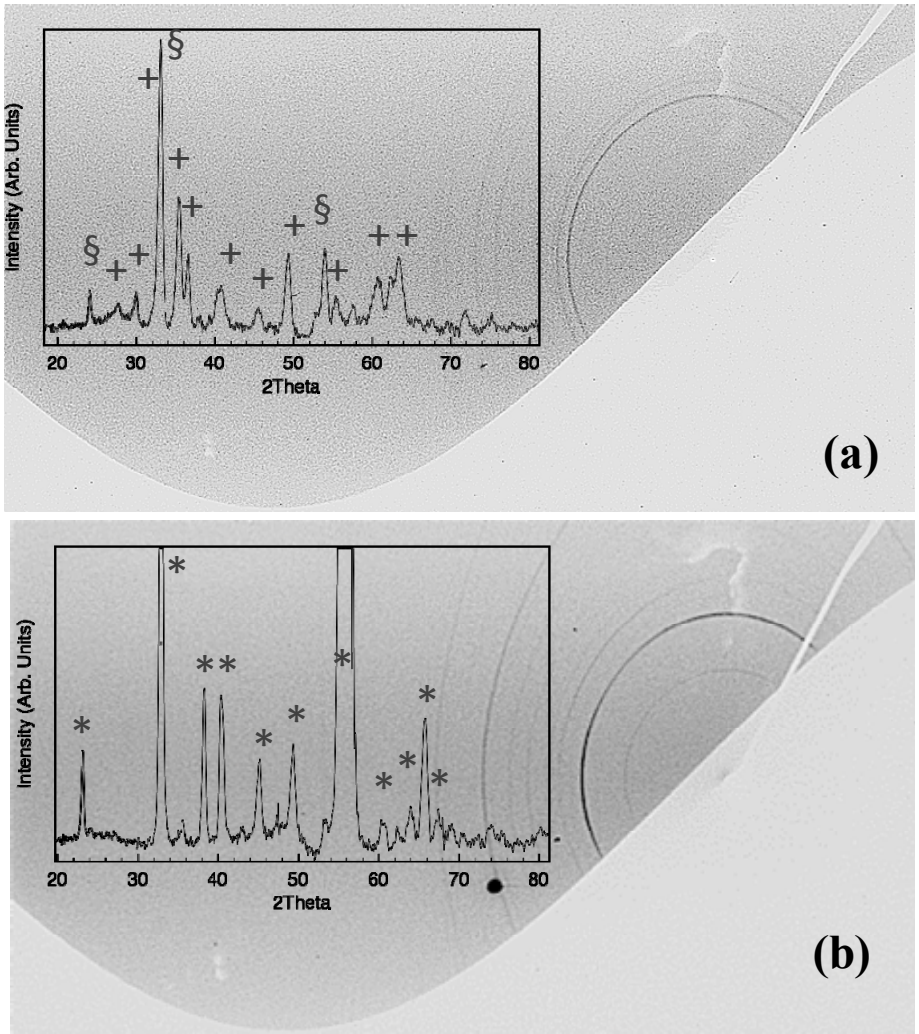

Fig. S1. XRD[2] images and conventional diffraction patterns for: (a) an ε-Fe_2O_3-based sample, grown on Si(100) under O_2 + H_2O atmosphere at 773 K; (b) a β-Fe_2O_3 sample, deposited on Si(100) under dry O_2 at 673 K. Reflections due to ε-, β- and α-Fe_2O_3 are marked by +, * and §,[R6] respectively.

Morphological characterization: FE-SEM analysis

Morphological analyses evidenced a significant dependence of the system features not only on the reaction atmosphere, but also on the selected growth temperature. In particular, the nanodeposit containing both ε- and α-Fe_2O_3 (obtained at 773 K) presented well interconnected agglomerates (Fig. S2a), giving rise to a compact system remarkably different from the nanorods observed for phase-pure ε-Fe_2O_3 (673 K, Fig. 2a). On other hand, the β-Fe_2O_3 nanodeposit obtained at 673 K (Fig. S2b) presented a morphology relatively similar to the homologous one produced at 773 K (Fig. 2b), apart from a lower thickness (400±20 *vs*. 650±30 nm).

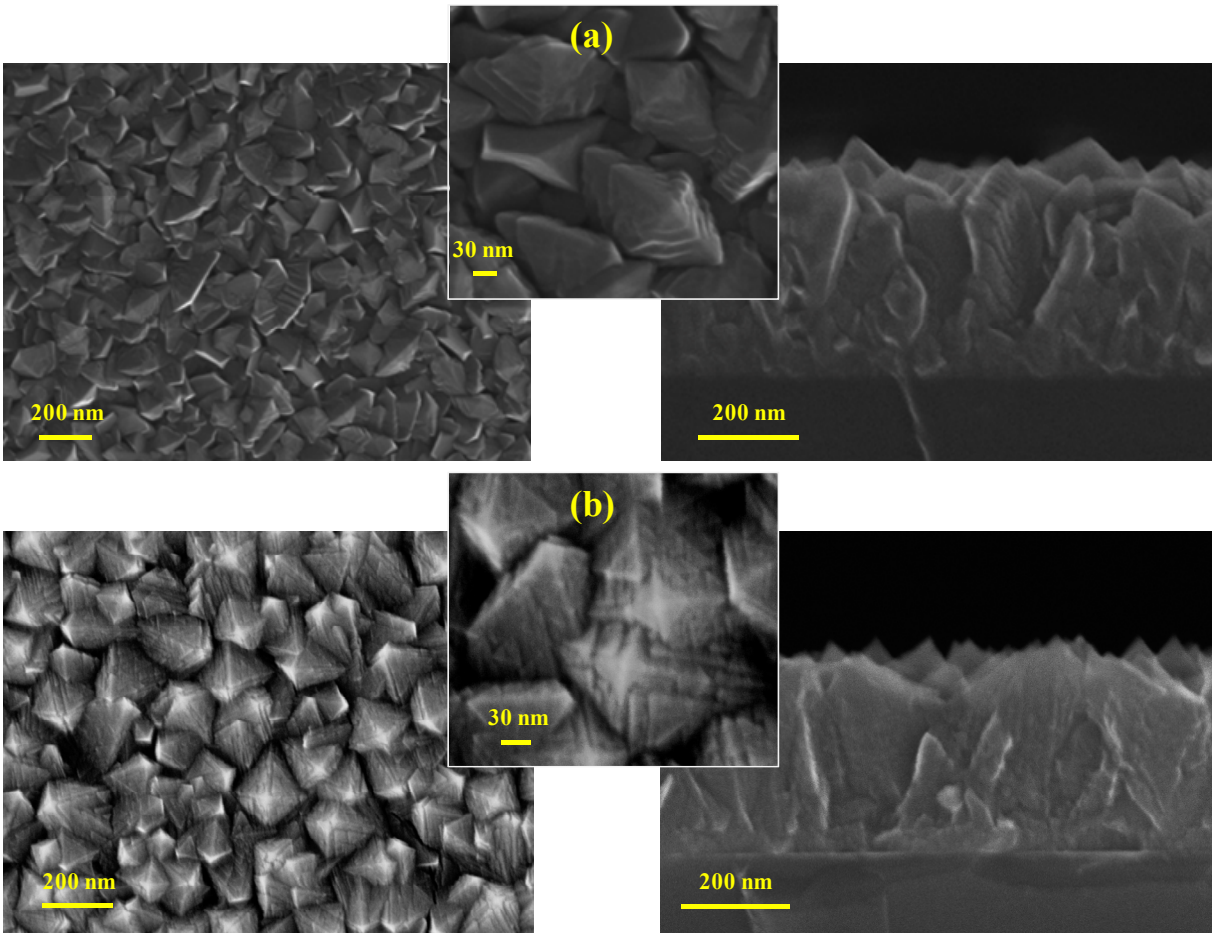

Fig. S2. Plane-view (left and centre pictures) and cross-sectional (right pictures) FE-SEM micrographs for (a) ε-Fe_2O_3 and (b) β-Fe_2O_3 nanomaterials, supported on Si(100). Growth conditions as in Fig. S1.

Compositional characterization: XPS analysis

The nanosystem chemical composition was investigated by XPS analysis, confirming the presence of iron(III) oxide. The presence of carbon (≈ 30 at. %) was related to surface contamination upon air exposure, since the C1s signal fell to noise level after a few minutes of Ar^+ erosion (4.5 kV, argon partial pressure = 5×10^{-8} mbar). No fluorine contamination was observed, confirming the clean decomposition of the adopted precursor into Fe_2O_3 under the present CVD conditions.

The Fe2p photoelectron peak (Fig. S3) presented two components, $Fe2p_{3/2}$ and $Fe2p_{1/2}$, with binding energies (BEs) of 711.2 and 725.0 eV (SI, Fig. S3), attributed to Fe(III) in Fe_2O_3.[R7,R8]

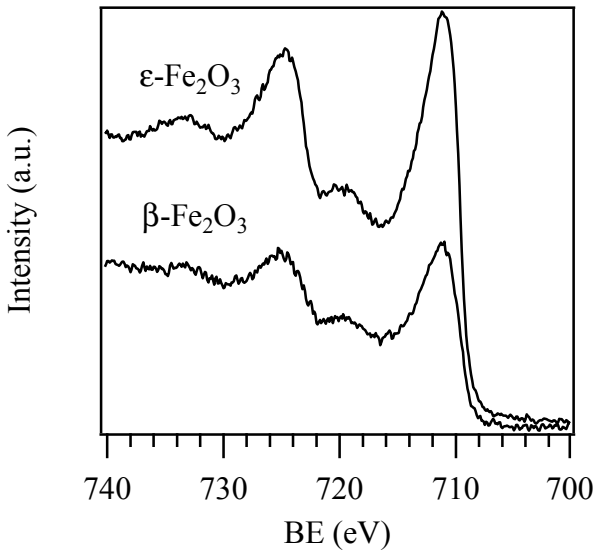

Fig. S3. Surface Fe2p photoelectron peaks for ε-Fe_2O_3 and β-Fe_2O_3 nanosystems deposited on Si(100) (growth conditions: O_2 + H_2O atmosphere, 673 K, and dry O_2 atmosphere, 773 K, respectively).

Irrespective of the phase composition, the surface O1s photopeak (Fig. S4) was fitted by two different bands. The peak (II), at BE = 531.9 eV could be attributed to the presence of absorbed hydroxyl/carbonates groups arising from atmospheric contamination, whereas a more intense signal

(I), at BE = 530.1 eV, corresponded to lattice oxygen from the Fe_2O_3 matrix.[R5,R6] Correspondingly, the surface O/Fe ratio (1.9) was higher than the expected stoichiometric value for Fe_2O_3.

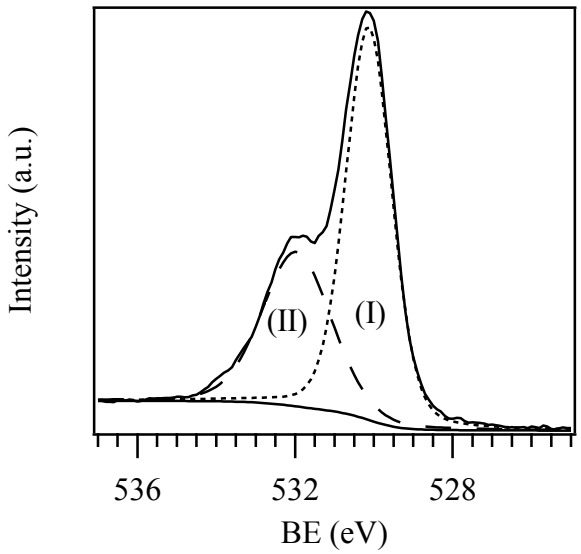

Fig. S4. Representative surface O1s photoelectron peaks for an ε-Fe_2O_3 sample deposited on Si(100) (growth conditions: O_2 + H_2O atmosphere, 673 K).

Magnetic measurements

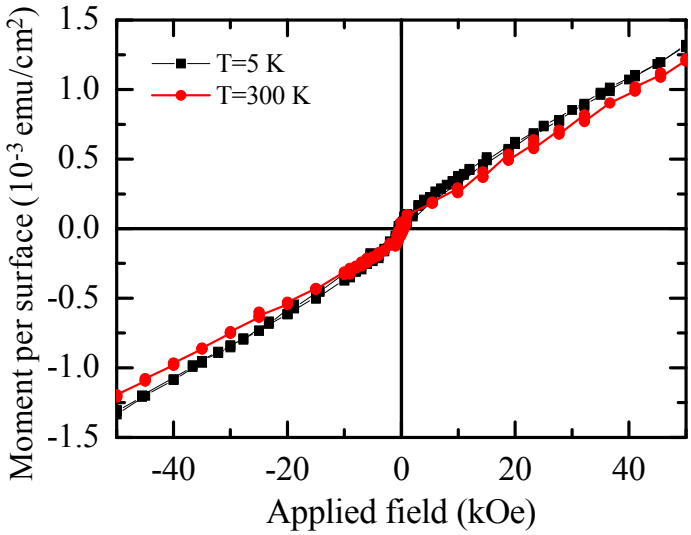

Fig. S5. Magnetic field dependence of the magnetization for phase-pure β-Fe_2O_3 nanosystems supported on Si(100) (growth conditions: dry O_2 atmosphere, 773 K) at 5 and 300 K. The magnetic field was applied parallel to the substrate surface.

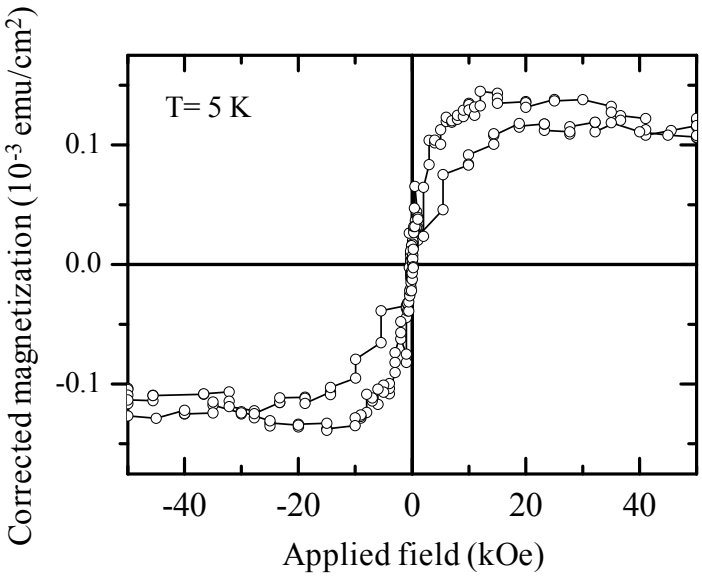

Fig. S6. Detail of the magnetic field dependence of the magnetization for phase-pure β-Fe_2O_3 nanosystems deposited on Si(100) (growth conditions as in Fig. S5) measured at 5 K after subtracting the high field linear contribution. The loop exhibits a coercive field of 0.5 kOe and is not closed up to 30 kOe, indicating the presence of few weak ferro- or ferrimagnetic nanoparticles in the present systems. The magnetic field was applied parallel to the substrate surface.

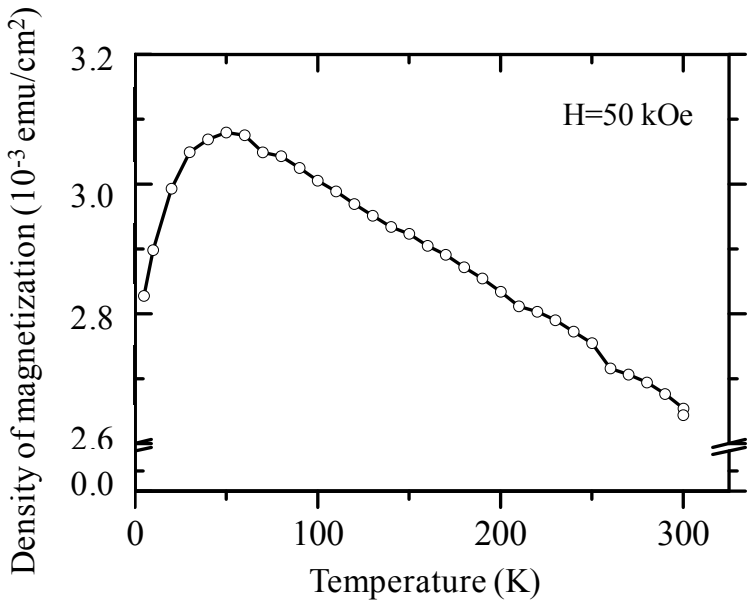

Fig. S7. Temperature dependence of the magnetization per unit surface of phase-pure ε-Fe_2O_3 nanosystems deposited on Si(100) (growth conditions as in Fig. S4), measured applying a magnetic field of 50 kOe parallel to the substrate surface.

References

R1 D. Barreca, G. Carraro, A. Devi, E. Fois, A. Gasparotto, R. Seraglia, C. Maccato, C. Sada, G. Tabacchi, E. Tondello, A.Venzo and M. Winter, *Dalton Trans.,* 2012, **41**, 149.

R2 D. Barreca, G. Carraro, A. Gasparotto, C. Maccato, R. Seraglia and G. Tabacchi, *Inorg. Chim. Acta,* 2012, **15**, 161.

R3 D. Barreca, A. Gasparotto, C. Maccato, E. Tondello, O. I. Lebedev and G. Van Tendeloo, *Cryst. Growth Des,*. 2009, **9**, 2470.

R4 Pattern n°51122, Inorganic Chemical Structure Database (ICSD), 2007.

R5 Pattern n°39-0238, International Centre for Diffraction Data Database (ICDD), 2007.

R6 Pattern n°33-0664, *International Centre for Diffraction Data Database* (ICDD), 2007.

R7 J. F. Moulder, W. F.Stickle, P. W. Sobol and K. D. Bomben, *Handbook of X-ray Photoelectron Spectroscopy*; Perkin-Elmer: Eden Prairie, MN, 1992.

R8 D. Barreca, G. A. Battiston, D. Berto, R. Gerbasi and E. Tondello, *Surf. Sci. Spectra,* 2001, **8**, 240.